

3 Introduction to Rheology and Application to Geophysics

C. Ancey

Cemagref, unité Erosion Torrentielle, Neige et Avalanches, Domaine Universitaire, 38402 Saint-Martin-d'Hères Cedex, France

3.1 Introduction

This chapter gives an overview of the major current issues in rheology through a series of different problems of particular relevance to geophysics. For each topic considered here, we will outline the key elements and point the reader toward the most helpful references and authoritative works. The reader is also referred to available books introducing rheology [1,2] for a more complete presentation and to the tutorial written by Middleton and Wilcock on mechanical and rheological applications in geophysics [3]. This chapter will focus on materials encountered by geophysicists (mud, snow, magma, etc.), although in most cases we will consider only suspensions of particles within an interstitial fluid without loss of generality. Other complex fluids such as polymeric liquids are rarely encountered in geophysics.

The mere description of what the term rheology embraces in terms of scientific areas is not easy. Roughly speaking, rheology distinguishes different areas and offshoots such as the following:

- *Rheometry*. The term “rheometry” is usually used to refer to a group of experimental techniques for investigating the rheological behavior of materials. It is of great importance in determining the constitutive equation of a fluid or in assessing the relevance of any proposed constitutive law. Most of the textbooks on rheology deal with rheometry. The books by Coleman, Markovitz, and Noll [4], Walters [5] and by Bird, Armstrong, and Hassager [6] provide a complete introduction to the viscometric theory used in rheometry for inferring the constitutive equation. Coussot and Ancey’s book [7] gives practical information concerning rheometrical measurements with natural fluids. Though primarily devoted to food processing engineering, Steffe’s book presents a detailed description of rheological measurements; a free sample is available on the web [8]. In Sect. 3.2, we will review the different techniques that are suitable to studying natural fluids. Emphasis is given both to describing the methods and the major experimental problems encountered with natural fluids.
- *Continuum mechanics*. The formulation of constitutive equations is probably the early goal of rheology. At the beginning of the 20th century, the non-Newtonian character of many fluids of practical interest motivated Professor Bingham to coin the term *rheology* and to define it as the study of the deformation and flow of matter. The development of a convenient mathemat-

ical framework occupied the attention of rheologists for a long time after the Second World War. At that time, theoreticians such as Coleman, Markovitz, Noll, Oldroyd, Reiner, Toupin, Truesdell, etc. sought to express rheological behavior through equations relating suitable variables and parameters representing the deformation and stress states. This gave rise to a large number of studies on the foundations of continuum mechanics [6]. Nowadays the work of these pioneers is pursued through the examination of new problems such as the treatment of multiphase systems or the development of nonlocal field theories. For examples of current developments and applications to geophysics, the reader may consult papers by Hutter and coworkers on the thermodynamically consistent continuum treatment of soil–water systems [9,10], the book by Vardoulakis and Sulem on soil failure [11], and Bedford and Dumheller’s review on suspensions [12]. A cursory glance at the literature on theoretical rheology may give the reader the impression that all this literature is merely an overly sophisticated mathematical description of the matter with little practical interest. In fact, excessive refinements in the tensorial expression of constitutive equations lead to prohibitive detail and thus substantially limit their utility or predictive capabilities. This probably explains why there is currently little research on this topic. Such limitations should not prevent the reader (and especially the newcomer) from studying the textbooks in theoretical rheology, notably to acquire the basic principles involved in formulating constitutive equations. Two simple problems related to these principles will be presented in Sect. 3.3 to illustrate the importance of an appropriate tensorial formulation of constitutive equations.

- *Rheophysics.* For many complex fluids of practical importance, bulk behavior is not easily outlined using a continuum approach. It may be useful to first examine what happens at a microscopic scale and then infer the bulk properties using an appropriate averaging process. Kinetic theories give a common example for gases [13] or polymeric liquids [6], which infer the constitutive equations by averaging all the pair interactions between particles. Such an approach is called *microrheology* or *rheophysics*. Here we prefer to use the latter term to emphasize that the formulation of constitutive equations is guided by a physical understanding of the origins of bulk behavior. Recent developments in geophysics are based on using kinetic theories to model bed load transport [14], floating broken ice fields [15], and rockfall and granular debris flows [16]. It is implicitly recognized that thoroughly modeling the microstructure would require prohibitive detail, especially for natural fluids. It follows that a compromise is generally sought between capturing the detailed physics at the particle level and providing applicable constitutive equations. Using dimensionless groups and approximating constitutive equations are commonly used operations for that purpose. In Sect. 3.4, we will consider suspensions of rigid particles within a Newtonian fluid to exemplify the different tools used in rheophysics. Typical examples of such fluids in a geophysical context include magma and mud. Chapters 4 and 14 provide further examples of rheophysical treatments with granular flows.

Other aspects of rheology, such as complex flow modeling and computational rheology, are not addressed in this introductory chapter. Chapter 2 in this book introduces the reader to the main rheological properties (viscoplasticity, time-dependent behaviour, etc.) encountered in geophysics. The reader is referred to examples of application to geophysical problems that are given in other chapters, notably Chap. 7 for lava flows, Chap. 13 for snow avalanches, Chaps. 22 and 21 for mud and debris flows.

3.2 Rheometry

At the very beginning, the term *rheometry* referred to a set of standard techniques for measuring shear viscosity. Then, with the rapid increase of interest in non-Newtonian fluids, other techniques for measuring the normal stresses and the elongational viscosity were developed. Nowadays, rheometry is usually understood as the area encompassing any technique which involves measuring mechanical or rheological properties of a material. This includes visualization techniques (such as photoelasticimetry for displaying stress distribution within a sheared material) or nonstandard methods (such as the slump test for evaluating the yield stress of a viscoplastic material). In most cases for applications in geophysics, shear viscosity is the primary variable characterizing the behavior of a fluid. Thus in the following, we will mainly address this issue, leaving aside all the problems related to the measurement of elongational viscosity. Likewise, the description of the most relevant procedures in rheometric measurement is not addressed here. We will first begin by outlining the main geometries used in rheometry. The principles underlying the viscometric treatment will be exposed in a simple case (flow down an inclined plane). Then, we will examine the most common problems encountered in rheometry. We will finish this section by providing a few examples of rheometric measurements, which can be obtained without a laboratory rheometer.

3.2.1 Standard viscometers

The basic principle of rheometry is to perform simple experiments where the flow characteristics such as the shear stress distribution and the velocity profile are known in advance and can be imposed. Under these conditions, it is possible to infer the *flow curve*, that is, the variation of the shear stress as a function of the shear rate, from measurements of flow quantities such as torque and the rotational velocity for a rotational viscometer. In fact, despite its apparent simplicity, putting this principle into practice for natural fluids raises many issues that we will discuss below. Most rheometers rely on the achievement of curvilinear (viscometric) flow [4]. The simplest curvilinear flow is the simple shear flow achieved by shearing a fluid between two plates in a way similar to Newton's experiment depicted in Sect. 3.3. But, in practice many problems (fluid recirculation, end effect, etc.) arise, which preclude using such a shearing box to obtain accurate measurements. Another simple configuration consists of an

inclined plane or channel. To exemplify the viscometric approach, we will show how some flow properties such as the *discharge equation* (variation of the fluid discharge as a function of the flow depth) can be used to infer the constitutive equation characteristics. We consider a gravity-driven free-surface flow in a steady uniform regime down an inclined channel. The plane is tilted at an inclination θ to the horizontal. We use the Cartesian coordinate system of origin 0 and of basis e_x, e_y, e_z , as depicted in Fig. 3.1.

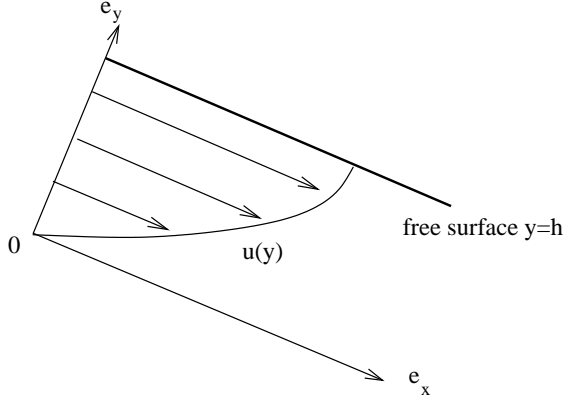


Fig. 3.1. Definition sketch for steady uniform flow

The velocity field \mathbf{u} only depends on the coordinate y and takes the following form: $u_x = u(y)$, $u_y = 0$, and $u_z = 0$, where u is a function of y to be determined. Accordingly, the strain-rate tensor $\dot{\boldsymbol{\gamma}} = (\nabla\mathbf{u} + {}^t\nabla\mathbf{u})/2$ has the following components in the coordinate system:

$$\dot{\boldsymbol{\gamma}} = \frac{\dot{\gamma}}{2} \begin{bmatrix} 0 & 1 & 0 \\ 1 & 0 & 0 \\ 0 & 0 & 0 \end{bmatrix}, \quad (3.1)$$

where the shear rate $\dot{\gamma}$ is defined as a function of the coordinate y and implicitly of the inclination θ : $\dot{\gamma}(y) = (\partial u / \partial y)_\theta$. The momentum balance can be written as:

$$\varrho \frac{d\mathbf{u}}{dt} = \varrho \mathbf{g} + \nabla \cdot \boldsymbol{\sigma}, \quad (3.2)$$

where ϱ and \mathbf{g} respectively denote the local material density and gravitational acceleration. We assume that there is no slip at the bottom: $u(y) = 0$. Furthermore, we assume that there is no interaction between the free surface and the ambient fluid above except the pressure exerted by the ambient fluid. Notably, we ignore surface tension effects on the free surface. Without restriction, the stress tensor can be written as the sum of a pressure term p and a deviatoric term called the extra-stress tensor \mathbf{s} (see also Sect. 3.3) [2,4]: $\boldsymbol{\sigma} = -p\mathbf{1} + \mathbf{s}$. For a homogeneous and isotropic simple fluid, the extra-stress tensor depends on the

strain rate only: $\mathbf{s} = G(\dot{\gamma})$, where G is a tensor-valued isotropic functional. In the present case, it is straightforward to show that the stress tensor must have the form:

$$\boldsymbol{\sigma} = -p\mathbf{1} + \begin{bmatrix} s_{xx} & s_{xy} & 0 \\ s_{xy} & s_{yy} & 0 \\ 0 & 0 & s_{zz} \end{bmatrix}. \quad (3.3)$$

Thus, the stress tensor is fully characterized by three functions: the shear stress $\tau = \sigma_{xy} = s_{xy}$, and the normal stress differences: $N_1 = s_{xx} - s_{yy}$ and $N_2 = s_{yy} - s_{zz}$, called the first and second normal stress differences, respectively. Since for steady flows acceleration vanishes and the components of \mathbf{s} only depend on y , the equations of motion (3.2) reduce to:

$$0 = \frac{\partial s_{xy}}{\partial y} - \frac{\partial p}{\partial x} + \rho g \sin \theta, \quad (3.4)$$

$$0 = \frac{\partial s_{yy}}{\partial y} - \frac{\partial p}{\partial y} - \rho g \cos \theta, \quad (3.5)$$

$$0 = \frac{\partial p}{\partial z}. \quad (3.6)$$

It follows from (3.6) that the pressure p is independent of z . Accordingly, integrating (3.5) between y and h implies that p must be written: $p(x, y) - p(x, h) = s_{yy}(y) - s_{yy}(h) + \rho g(h - y) \cos \theta$. It is possible to express (3.4) in the following form:

$$\frac{\partial}{\partial y} (s_{xy} + \rho g y \sin \theta) = \frac{\partial p(x, h)}{\partial x}. \quad (3.7)$$

Equation (3.7) has a solution only if both terms of this equation are equal to a function of z , which we denote $b(z)$. Moreover, (3.6) implies that $b(z)$ is actually independent of z ; thus, in the following we will note: $b(z) = b$. The solutions to (3.7) are: $p(x, h) = bx + c$ and $s_{xy}(h) - s_{xy}(y) - \rho g y \sin \theta = b(h - y)$, where c is a constant, which we will determine. To that end, let us consider the free surface. It is reasonable and usual to assume that the ambient fluid friction is negligible. The stress continuity at the interface implies that the ambient fluid pressure p_0 exerted on an elementary surface at $y = h$ (oriented by \mathbf{e}_y) must equal the stress exerted by the fluid. Henceforth, the boundary conditions at the free surface may be expressed as: $-p_0\mathbf{e}_y = \boldsymbol{\sigma}\mathbf{e}_y$, which implies in turn that: $s_{xy}(h) = 0$ and $p_0 = p(x, h) - s_{yy}(h)$. Comparing these equations to former forms leads to $b = 0$ and $c = p_0 + s_{yy}(h)$. Accordingly, we obtain for the shear and normal stress distributions:

$$\tau = \rho g(h - y) \sin \theta, \quad (3.8)$$

$$\sigma_{yy} = s_{yy} - (p - p_0) = -\rho g(h - y) \cos \theta. \quad (3.9)$$

The shear and normal stress profiles are determined regardless of the form of the constitutive equation. For simple fluids, the shear stress is a one-to-one function of the shear rate: $\tau = f(\dot{\gamma})$. Using the shear stress distribution (3.8) and the

inverse function f^{-1} , we find: $\dot{\gamma} = f^{-1}(\tau)$. A double integration leads to the flow rate (per unit width):

$$q = \int_0^h dy \int_0^y f^{-1}(\tau(\xi)) d\xi . \quad (3.10)$$

Taking the partial derivative of q with respect to h , we obtain:

$$\dot{\gamma} = f^{-1}(\tau(h)) = \frac{1}{h} \left(\frac{\partial q}{\partial h} \right)_\theta . \quad (3.11)$$

This relation allows us to directly use a channel as a rheometer. The other normal components of the stress tensor cannot be easily measured. The curvature of the free surface of a channeled flow may give some indication of the first normal stress difference. Let us imagine the case where it is not equal to zero. Substituting the normal component s_{yy} by $s_{yy} = s_{xx} - N_1$ in (3.5), then integrating, we find:

$$s_{xx} = p + \rho g y \cos \theta + N_1 + d , \quad (3.12)$$

where d is a constant. Imagine that a flow section is isolated from the rest of the flow and the adjacent parts are removed. In order to hold the free surface flat (it will be given by the equation $y = h, \forall z$), the normal component σ_{xx} must vary and balance the variations of N_1 due to the presence of the sidewalls (for a given depth, the shear rate is higher in the vicinity of the wall than in the center). But at the free surface, the boundary condition forces the normal stress σ_{xx} to vanish and the free surface to bulge out. To first order, the free surface equation is:

$$-\rho g y \cos \theta = N_1 + d + \mathcal{O}(y) . \quad (3.13)$$

If the first normal stress difference vanishes, the boundary condition $-p_0 \mathbf{e}_y = \boldsymbol{\sigma} \mathbf{e}_y$ is automatically satisfied and the free surface is flat. In the case where the first normal stress difference does not depend on the shear rate, there is no curvature of the shear free surface. The observation of the free surface may be seen as a practical test to examine the existence and sign of the first normal stress difference and to quantify it by measuring both the velocity profile at the free surface and the free-surface equation. Computation of the shear-stress function and normal stress differences is very similar for other types of viscometers. Figure 3.2 reports the corresponding functions for the most common viscometers. All these techniques are robust and provide accurate measurements for classic fluids, with uncertainty usually less than 2%. For geophysical fluids, many problems of various types may arise.

First, the viscometric treatment relies on the crucial assumption that the extra-stress tensor is a one-to-one function of the strain-rate tensor only (class of simple fluids). Many classes of material studied in geophysics are not in fact homogeneous, isotropic, or merely expressible in the form $\boldsymbol{\sigma} = -p\mathbf{1} + \mathbf{s}(\dot{\boldsymbol{\gamma}})$. For instance, for materials with time-dependent properties (thixotropic materials, viscoelastic materials), the constitutive equation can be expressed in the form $\boldsymbol{\sigma} = -p\mathbf{1} + \mathbf{s}(\dot{\boldsymbol{\gamma}})$ only for a steady state. Another example is provided by granular

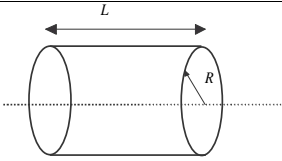
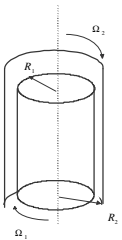
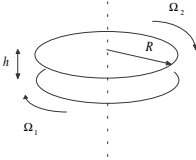
Rheometer type	Sketch	Viscometric function
Capillary tube (Poiseuille flow)		$\dot{\gamma} \approx \lambda \left(\frac{\Delta p_g}{L} \frac{R}{2} \right) = \frac{1}{\pi \alpha^2 R^3} \frac{\partial (q \alpha^3)}{\partial \alpha}$ $\alpha = \frac{\Delta p_g}{L} \quad (\text{pressure variation per unit length})$ <p>q: flow rate, Δp_g: applied pressure gradient</p>
Concentric cylinder (Couette flow)		$\Delta \Omega = \Omega_2 - \Omega_1 = \frac{1}{2} \int_{C/(2\pi R_1^2)}^{C/(2\pi R_2^2)} \dot{\gamma}(\tau) d \ln \tau$ $\tau = \frac{C}{2\pi R_1^2}$ <p>R_1: inner radius; R_2: outer radius C: torque (per unit height)</p>
Parallel-plate		$\dot{\gamma} \approx R \frac{\Delta \Omega}{h}, \quad C = \frac{M}{2\pi R^3}, \quad \Delta \Omega = \Omega_2 - \Omega_1$ $\tau = C \left(3 + \frac{\partial \ln C}{\partial \ln \dot{\gamma}} \right)$ <p>M: measured torque</p>
Inclined plane	See Fig. 1	$\tau = \rho g h \sin \theta$ $\dot{\gamma} = \frac{1}{h} \left(\frac{\partial q}{\partial h} \right)$

Fig. 3.2. Chief geometries used in rheometry

flows. In this case, when applied to experimental data obtained by studying dry granular flows down an inclined channel [17], the viscometric treatment leads to the conclusion that the flow curve should be a decreasing function of the shear rate in violation of a stability criterion imposing that the flow curve be an increasing function. Although such a decrease in the flow curve cannot be directly interpreted in terms of a constitutive equation, it provides interesting rheological information that can be explained on the basis of microstructural theories [18].

Second, for most viscometers, computing the shear rate from experimental data can raise serious problems. A major source of uncertainty is that in most viscometric procedures the shear rate is expressed as a derivative – for instance $\partial q / \partial h$ in (3.11) – which must be estimated from experimental data. To do so, different procedures are available but they do not always provide the same results, especially when data are noisy [19]. A typical example of these problems

is given by the concentric-cylinder rheometer (or Couette rheometer). The shear rate is inferred from the rotational velocity Ω and the torque (per unit depth) C using the following relationship:

$$\Omega = -\frac{1}{2} \int_{C/(2\pi R_1^2)}^{C/(2\pi R_2^2)} \dot{\gamma}(\tau) d(\ln \tau). \quad (3.14)$$

When the gap between the two cylinders is narrow, it is possible to approximate the shear rate as: $\dot{\gamma} = R_1\Omega/(R_2 - R_1) + \mathcal{O}(1 - R_2/R_1)$. However, such a geometry is not very suitable to studying natural fluids (slipping, size effects, etc.) and usually a large gap is preferred. For large gaps, one of the most common approximations is attributed to Krieger who proposed for Newtonian and power-law fluids [20,21]:

$$\dot{\gamma} = \frac{2\Omega(1 + \alpha)}{1 - \beta f} f \quad (3.15)$$

with $f = d \ln \Omega / d \ln C$; $\alpha = f' f^{-2} \chi_1(-f \log \beta)$; $\chi_1(x) = x(xe^x - 2e^x + x + 2)(e^x - 1)^{-2}/2$, $\beta = (R_1/R_2)^2$. However, this method can give poor results with yield stress fluids, especially if it is partially sheared within the gap. In this case, Nguyen and Boger [22] have proposed using $\dot{\gamma} = 2\Omega d \ln \Omega / d \ln C$. In their treatment of debris suspensions, Coussot and Piau [23] used an alternative consisting of an expansion into a power series of (3.15). They obtained: $\dot{\gamma} = 2\Omega \sum_{n=0}^{\infty} f(\beta^n C / (2\pi R_1^2))$. For methods of this kind, computing the shear rate requires specifying the type of constitutive equation in advance. Furthermore, depending on the procedure chosen, uncertainty on the final results may be as high as 20% or more for natural fluids. Recently, a more effective and practical method of solving the inverse problem has been proposed [24,25]: the procedure based on Tikhonov regularization does not require the algebraic form of the $\tau - \dot{\gamma}$ curve to be prespecified and has the advantage of filtering out noise. The only viscometer that poses no problem in converting experimental data into a $\tau - \dot{\gamma}$ curve is the parallel-plate rheometer. In this case, the shear rate distribution is imposed by the operator: $\dot{\gamma} = \Omega R/h$. But such a relationship holds provided centrifugal forces are negligible compared to the second normal stress difference: $\rho R^2 w^2 \ll N_2$, where w is the orthoradial component of the velocity. Such an effect can be detected experimentally either by observing secondary flows or by noticing that doubling both the gap and the rotational velocity (thus keeping the shear rate constant) produces a significant variation in the measured torque.

Third, any rheometer is subjected to end effects, which have to be corrected or taken into account in the computation of the flow curve. For instance, end effects in a channel are due to the finite length of the channel as well as the sidewalls, both producing potentially significant variations in the flow depth. Likewise, in a Couette rheometer, the measured torque includes a contribution due to the shearing over the bottom surface of the bob. Such a contribution is substantially reduced using a bob with a hole hollowed on the bottom surface so that air is trapped when the bob is immersed in the fluid. But this can be inefficient for natural fluids, such as debris suspensions, and in this case, the

bottom contribution to the resulting torque must be directly assessed using the method proposed by Barnes and Carnali [26]. For a parallel-plate rheometer, the fluid surface at the peripheral free surface may bulge out or creep, inducing a significant variation in the measured torque, possibly varying with time. Furthermore, many natural fluids encountered in geophysics are suspensions with a large size distribution. The size of the rheometer should be determined such that its typical size (e.g. the gap in a rotational viscometer) is much larger than the largest particle size. For instance, for debris flows, this involves using large-sized rheometers [23,27].

Last, many disturbing effects may arise. They often reflect the influence of the microstructure. For instance, for a particle suspension, especially made up of nonbuoyant particles, sedimentation and migration of particles can significantly alter the stress distribution and thus the measured torque. Likewise, for concentrated pastes, a fracture inside the sheared sample may sometimes be observed, usually resulting from a localization of shear within a thin layer. Other disturbing effects are experimental problems pertaining to the rheometer type. For instance, when using a rotational viscometer with a smooth metallic shearing surface, wall slip can occur. Apart from effects resulting from microstructural changes, which are a part of the problem to study, it is sometimes possible to reduce disturbing effects or to account for them in the flow-curve computation. For instance, to limit wall slip, the shearing surfaces can be roughened. Another strategy involves measuring the slipping velocity directly and then computing an effective shear rate. Still another possibility requires using the same rheometer with different sizes, as first proposed by Mooney for the capillary rheometer.

All the above issues show that, for complex fluids (the general case for natural fluids studied in geophysics), rheometry is far from being an ensemble of simple and ready-for-use techniques. On the contrary, investigating the rheological properties of a natural material generally requires many trials using different rheometers and procedures. In some cases, visualization techniques (such as nuclear magnetic resonance imagery, transparent interstitial fluid and tools, birefringence techniques) may be helpful to monitor microstructure changes. Most of the commercialized rheometers are now controlled by a PC-type computer, both controlling the measurements and providing automatic procedures for computing the flow curve. Such procedures should be reserved for materials whose rheological behavior is well known, and consequently are of limited interest for natural fluids.

3.2.2 What Can Be Done Without a Rheometer?

In the laboratory, it is frequently impossible to investigate the rheological properties of a natural fluid using a rheometer. For instance, with snow or magma, such tests are almost always impractical. For debris suspensions, it is usually impossible to carry out measurements with the complete range of particle size. This has motivated researchers to develop approximate rheometric procedures and to investigate the relations between field observations and rheological properties. For instance, given the sole objective of determining the yield stress, the

semiempirical method referred to as a *slump test* can provide an estimate of the yield stress for a viscoplastic material. This method involves filling a cylinder with the material to be tested, lifting the cylinder off and allowing the material to flow under its own weight. The profile of the final mound of material as well as the difference δ between the initial and final heights is linked to the yield stress. Pashias and Boger [28] have found:

$$\frac{\delta}{h} = 1 - 2 \frac{\tau_c}{\rho gh} \left[1 - \ln \left(2 \frac{\tau_c}{\rho gh} \right) \right], \quad (3.16)$$

where h is the cylinder height, ρ the material density. Close examination of experimental data published by Pashias and Boger shows a deviation from the theoretical curve for yield stress values in excess of approximately $0.15\rho gh$. For yield stress values lower than $0.15\rho gh$ (or for $\delta/h > 0.4$), uncertainty was less than 10% for their tests. The explanation of the deviation for higher yield stress values lies perhaps in the weakness of the assumption on the elastoplastic behavior for very cohesive materials. Coussot, Proust and Ancey [29] developed an alternative approach based on an interpretation of the deposit shape. They showed that the free surface profile (the relationship between the material height y and the distance from the edge x) depends on the yield stress only. On a flat horizontal surface, the free surface profile has the following expression:

$$\frac{\rho gy}{\tau_c} = \sqrt{2 \frac{\rho gx}{\tau_c}}. \quad (3.17)$$

Comparisons between rheological data deduced from a parallel plate rheometer and free surface profile measurements showed an acceptable agreement for fine mud suspensions and debris flow materials. Uncertainty was less than 20%, within the boundaries of acceptable uncertainty for rheometrical measurement. The major restriction in the use of (3.17) stems from the long-wave approximation, which implies that the mound height must far outweigh the extension of the deposit: $h - \delta \gg \tau_c/(\rho g)$. The method proposed by Coussot et al. [29] can be extended to different rheologies and boundary conditions. In the field, such a method applied to levee profiles of debris flow can provide estimates of the bulk yield stress provided that the assumption of viscoplastic behavior holds.

Observing and interpreting natural deposits may provide interesting information either on the flow conditions or rheological features of the materials involved [30]. For instance, laboratory experiments performed by Pouliquen with granular flows have shown that the flow features (e.g. the mean velocity) of a dry granular free-surface unconfined flow can be related to the final thickness of the deposit [31]. Although fully developed in the laboratory, such a method should be applicable to natural events involving granular flows. More evidence of the interplay between the deposit shape, the flow conditions, and the rheological features is given by the height difference of two lateral levees deposited by a debris flow in a bending track [32].

3.3 The Contribution of Continuum Mechanics

In 1687, Isaac Newton proposed that “the resistance which arises from the lack of slipperiness of the parts of the liquid, other things being equal, is proportional to the velocity with which the parts of the liquid are separated from one another” [33]. This forms the basic statement behind the theory of Newtonian fluid mechanics. Translated into modern scientific terms, this sentence means that the resistance to flow (per unit area) τ is proportional to the velocity gradient U/h :

$$\tau = \mu \frac{U}{h}, \quad (3.18)$$

where U is the relative velocity with which the upper plate moves and h is the thickness of fluid separating the two plates (see Fig. 3.3). μ is a coefficient intrinsic to the material, which is termed *viscosity*. This relationship is of great practical importance for many reasons. It is the simplest way of expressing the constitutive equation for a fluid (linear behavior) and it provides a convenient experimental method for measuring the constitutive parameter μ by measuring the shear stress exerted by the fluid on the upper plate moving with a velocity U (or conversely by measuring the velocity when a given tangential force is applied to the upper plate).

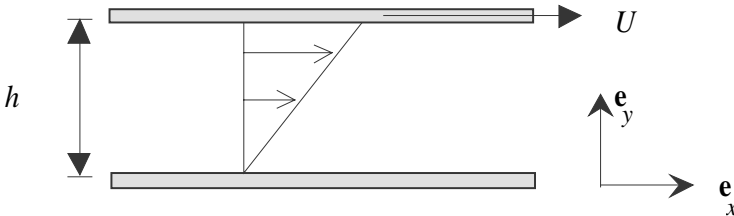


Fig. 3.3. Illustration of a fluid sheared by a moving upper plate

In 1904, Trouton did experiments on mineral pitch involving stretching the fluid with a given velocity [34]. Figure 3.4 depicts the principle of this experiment. The fluid undergoes a uniaxial elongation achieved with a constant elongation rate $\dot{\alpha}$, defined as the relative deformation rate: $\dot{\alpha} = \dot{l}/l$, where l is the fluid sample length. For his experiments, Trouton found a linear relationship between the applied force per unit area σ and the elongation rate:

$$\sigma = \mu_e \alpha = \mu_e \frac{1}{l} \frac{dl}{dt}. \quad (3.19)$$

This relationship was structurally very similar to the one proposed by Newton but it introduced a new material parameter, which is now called *Trouton viscosity*. This constitutive parameter was found to be three times greater than the Newtonian viscosity inferred from steady simple-shear experiments: $\mu_e = 3\mu$.

At first glance, this result is both comforting since behavior is still linear (the resulting stress varies linearly with the applied strain rate) and disturbing since the value of the linearity coefficient depends on the type of experiment. In fact, Trouton's result does not lead to a paradox if we are careful to express the constitutive parameter in a tensorial form rather than a purely scalar form.

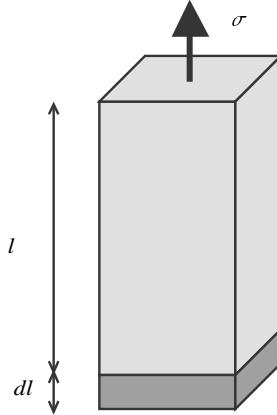


Fig. 3.4. Typical deformation of a material experiencing a normal stress σ

This was achieved by Navier and Stokes, who independently developed a consistent three-dimensional theory for Newtonian viscous fluids. For a simple fluid, the stress tensor $\boldsymbol{\sigma}$ can be cast in the following form:

$$\boldsymbol{\sigma} = -p\mathbf{1} + \mathbf{s} \quad (3.20)$$

where p is called the *fluid pressure* and \mathbf{s} is the extra-stress tensor representing the stresses resulting from a relative motion within the fluid. It is also called the *deviatoric stress tensor* since it represents the departure from equilibrium. The pressure p is defined as (minus) the average of the three normal stresses $p = -\text{tr } \boldsymbol{\sigma}/3$. This also implies that $\text{tr } \mathbf{s} = 0$. The pressure used in (3.20) is analogous to the static fluid-pressure in the sense that it is a measure of the local intensity of the squeezing of the fluid. Contrary to the situation for fluids at rest, the connection between this purely mechanical definition and the term pressure used in thermodynamics is not simple. For a Newtonian viscous fluid, the Navier–Stokes equation postulates that the extra-stress tensor is linearly linked to the strain rate tensor $\dot{\boldsymbol{\gamma}} = (\nabla\mathbf{u} + {}^t\nabla\mathbf{u})/2$ (where \mathbf{u} is the local fluid velocity):

$$\mathbf{s} = 2\eta\dot{\boldsymbol{\gamma}} \quad (3.21)$$

where η is called the Newtonian viscosity. It is worth noticing that the constitutive equation is expressed as a relationship between the extra-stress tensor and the local properties of the fluid, which are assumed to depend only on the

instantaneous distribution of velocity (more precisely, on the departure from uniformity of that distribution). There are many arguments from continuum mechanics and analysis of molecular transport of momentum in fluids, which show that the local velocity gradient $\nabla \mathbf{u}$ is the parameter of the flow field with most relevance to the deviatoric stress (see [37]). On the contrary, the pressure is not a constitutive parameter of the moving fluid. When the fluid is compressible, the pressure p can be inferred from the free energy, but it is indeterminate for incompressible Newtonian fluids. If we return to the previous experiments, we infer from the momentum equation that the velocity field is linear : $\mathbf{u} = U \mathbf{e}_x y/h$. We easily infer that the shear rate is: $\dot{\gamma} = \partial u/\partial y = U/h$ and then comparing (3.21) to (3.18) leads to: $\eta = \mu$. Thus, the Newtonian viscosity corresponds to the simple shear viscosity. In the case of a uniaxial elongation, the components of the strain-rate tensor are:

$$\dot{\gamma} = \begin{bmatrix} \dot{\alpha} & 0 & 0 \\ 0 & -\dot{\alpha}/2 & 0 \\ 0 & 0 & -\dot{\alpha}/2 \end{bmatrix} . \quad (3.22)$$

At the same time, the stress tensor can be written as:

$$\boldsymbol{\sigma} = \begin{bmatrix} \sigma & 0 & 0 \\ 0 & 0 & 0 \\ 0 & 0 & 0 \end{bmatrix} . \quad (3.23)$$

Comparing (3.20), (3.22), and (3.23) leads to: $p = -\eta \dot{\alpha}$ and $\sigma = 3\eta \dot{\alpha}$, that is: $\mu_e = 3\eta$, confirming that the Trouton elongational viscosity is three times greater than the viscosity. It turns out that Trouton's and Newton's experiments reflect the same constitutive behavior. This example shows the importance of an appropriate tensorial form for expressing the stress tensor. In the present case, the tensorial form (3.21) may be seen as a simple generalization of the simple shear expression (3.18).

In many cases, most of the available information on the rheological behavior of a material is inferred from simple shear experiments (see Sect. 3.2). But, contrary to the Newtonian (linear) case, the tensorial form cannot be merely and easily generalized from the scalar expression fitted to experimental data. First, building a three-dimensional expression of the stress tensor involves respecting a certain number of formulation principles. These principles simply express the idea that the material properties of a fluid should be independent of the observer or frame of reference (principle of material objectivity) and the behavior of a material element depends only on the previous history of that element and not on the state of neighboring elements [6]. Then it is often necessary to provide extra information or rules to build a convenient expression for the constitutive equation. To illustrate this, we shall consider a simple example: the Bingham equation (see also Chaps. 2 and 22). When a fluid exhibits viscoplastic properties, we usually fit experimental data with a Bingham equation as a first approximation [35,36,38]:

$$\dot{\gamma} > 0 \Rightarrow \tau = \tau_c + K \dot{\gamma} . \quad (3.24)$$

Equation (3.24) means that for shear stresses in excess of a critical value, called the *yield stress*, the shear stress is a linear function of the shear rate. Conversely when $\tau \leq \tau_c$ there is no shear within the fluid ($\dot{\gamma} = 0$). The question arises as to how the scalar expression can be transformed into a tensorial form. The usual but not the only way is to consider a process, called *plastic rule*, as the key process of yielding. A plastic rule includes two ingredients. First, it postulates the existence of a surface in the stress space ($\sigma_1, \sigma_2, \sigma_3$) delimiting two possible mechanical states of a material element (σ_i denotes a principal stress, that is an eigenvalue of the stress tensor) as depicted in Fig. 3.5. The surface is referred to as the *yield surface* and is usually represented by an equation in the form $f(\sigma_1, \sigma_2, \sigma_3) = 0$. When $f < 0$, behavior is generally assumed to be elastic or rigid. When $f = 0$, the material yields. Second it is assumed that, after yielding, the strain-rate is directly proportional to the surplus of stress, that is, the distance between the point the representing the stress state and the yield surface. Translated into mathematical terms, this leads to write: $\dot{\boldsymbol{\gamma}} = \lambda \nabla f$ with λ a proportionality coefficient (Lagrangian multiplier).

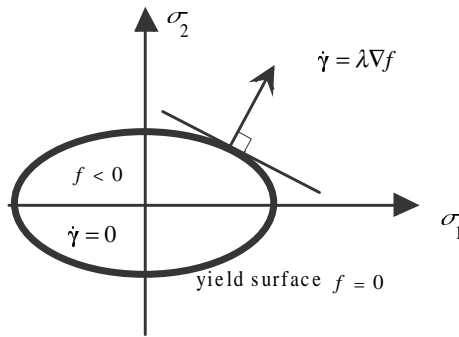


Fig. 3.5. Yield surface delimiting two domains

How must the yield function f be built to satisfy the principle of material objectivity? For f to be independent of the frame, it must be expressed not as a function of the components of the stress but as a function of its invariants. An *invariant* is a quantity that does not depend on the frame in which it is expressed. For instance, it is well known that the determinant of a tensor is an invariant. In contrast with tensor invariants used in mathematics without physical meaning, it is usual in mechanics to use specific forms for the invariants of the stress tensor: they are defined in such a way that they can be used as the coordinates of the point representing the stress state M in the stress space (see Fig. 3.6). The first invariant $I_1 = \text{tr } \boldsymbol{\sigma} = \sigma_1 + \sigma_2 + \sigma_3$ represents the *mean stress* multiplied by 3 ($|\mathbf{OP}| = I_1/3$ in Fig. 3.6), the second invariant $I_2 = (\text{tr}^2 \boldsymbol{\sigma} - \text{tr } \boldsymbol{\sigma}^2)/2 = -\text{tr}(\mathbf{s}^2)/2$ can be interpreted as the deviation of a stress state from the mean stress state ($|\mathbf{PM}|^2 = -2I_2$ in Fig. 3.6) and is accordingly called the *stress deviator*. The third invariant $I_3 = -\text{tr } \mathbf{s}^3/6$ reflects the angle in the deviatoric plane made by

the direction PM with respect to the projection of σ_1 -axis and is sometimes called the *phase* ($\cos^2 3\varphi = I_3^2/I_2^3$ in Fig. 3.6).

If the material is an isotropic and homogenous fluid, the yield function f is expected to be independent of the mean pressure and the third invariant (for reasons analogous to those given above for explaining the form of the constitutive equation). Thus we have $f(\sigma_1, \sigma_2, \sigma_3) = f(I_2)$. In plasticity, the simplest yield criterion is the von Mises criterion, asserting that yield occurs whenever the deviator exceeds a critical value (whose root gives the yield stress): $f(I_2) = \sqrt{-I_2} - \tau_c$. As depicted in Fig. 3.6, the resulting yield surface is a cylinder of radius τ_c centered around an axis $\sigma_1 = \sigma_2 = \sigma_3$. (If we draw the yield surface in the extra-stress space, we obtain a sphere of radius $\sqrt{2}\tau_c$.)

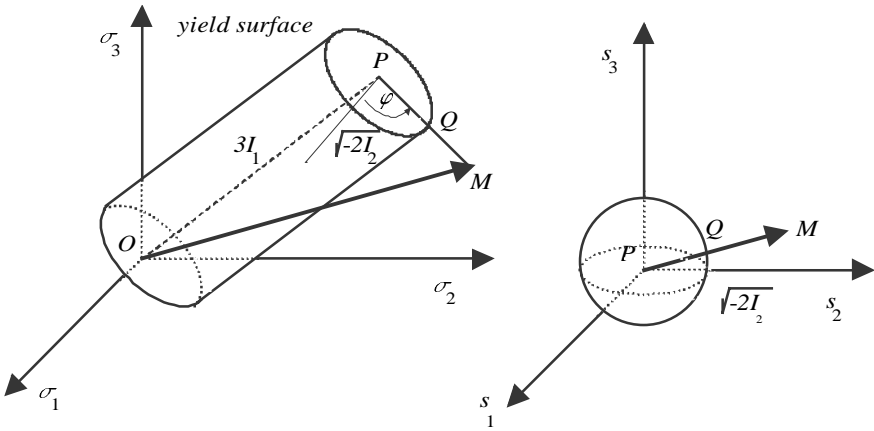


Fig. 3.6. On the left, the yield surface in the stress space when the von Mises criterion is selected as yield function. A stress state is characterized by its three principal stresses and thus can be reported in the stress space. The three invariants of the stress tensor can be interpreted in terms of coordinates

Once the stress state is outside the cylinder defined by the yield surface, a flow occurs within the material. As stated above, it is assumed that the strain rate is proportional to the surplus of stress. This leads to the expression:

$$\dot{\gamma} = \lambda \partial f / \partial \mathbf{s} = \lambda \left(\sqrt{-I_2} - \tau_c \right) \frac{\mathbf{s}}{\sqrt{-I_2}}. \tag{3.25}$$

For convenience, we define the proportionality coefficient as: $\lambda^{-1} = 2\eta$. It is generally more usual to express the constitutive equation in the converse form $\mathbf{s}(\dot{\gamma})$. To that end, we express the second invariant of the strain rate tensor J_2 as $J_2 = -\text{tr}(\dot{\gamma}^2)/2 = [\lambda (\sqrt{-I_2} - \tau_c)]^2$. Then we deduce:

$$\dot{\gamma} = 0 \Leftrightarrow \sqrt{-I_2} \leq \tau_c, \tag{3.26}$$

$$\dot{\gamma} \neq 0 \Leftrightarrow \boldsymbol{\sigma} = -p\mathbf{1} + \left(2\eta + \frac{\tau_c}{\sqrt{-J_2}} \right) \dot{\boldsymbol{\gamma}}, \quad (3.27)$$

which is the usual form of the Bingham constitutive equation. It is worth noting that contrary to the Newtonian case, the general tensorial expression (3.26)–(3.27) cannot not easily be extrapolated from the steady simple-shear equation (3.24).

3.4 Rheophysics

The rheophysical approach seeks to derive the bulk properties by examining what may happen at the microscopic scale. Generally the bulk stress tensor is computed by averaging the local stresses. Accurate computation has been achieved in a certain number of simple cases. Kinetic theories for gases, polymers, and granular media (rapidly sheared) are typical examples. In most cases for fluids involved in geophysics, computations are so much more complex that analytical results cannot be provided. One can, however, benefit from this approach either by building approximate rheological models or by finding convenient scalings for the key variables describing bulk behavior. Typical examples include all the treatments focusing on the rheology of concentrated suspensions. To begin with, we will outline the principles used in deriving the bulk constitutive equations. This will lead to introducing important concepts such as the *pair distribution function*, the *averaging operator*, *particle interactions*, and *evolution equations*. We will examine these different notions through the example of Newtonian suspensions with no loss of generality since they can be encountered with a similar meaning in other theories such as the kinetic theories for granular flows [39]. Then we will examine how it is possible to simplify the constitutive equation to obtain approximate equations. The last subsection will demonstrate the advantages of dimensional analysis combined with a microstructural analysis of particle interactions in deriving appropriate scalings for experimental data and theoretical results.

3.4.1 Definition of the Bulk Stress Tensor and Selected Applications

One of the key questions in rheophysics is to establish the way in which bulk behavior can be deduced from the microstructure properties. For suspensions, this is generally achieved by averaging the local stress and particle interactions. As all the issues around the most appropriate averaging procedure are still being debated, here we restrict our attention to the approach followed by Batchelor and many subsequent authors. The reader interested in further information on averaging is referred to specific papers [41,42,43,44,45,46,47,48,40].

In the following, we consider a suspension of rigid spherical particles of radius a within an incompressible Newtonian fluid with viscosity η . Particles are assumed to be identical and neutrally buoyant. The solid fraction ϕ is defined as the ratio of the solid volume to the total volume. In a fundamental paper,

Batchelor showed that the bulk stress is the sum of a fluid contribution and a particle contribution [49]:

$$\bar{\boldsymbol{\sigma}} = \bar{\boldsymbol{\sigma}}^{(f)} + \bar{\boldsymbol{\sigma}}^{(p)}, \quad (3.28)$$

where the fluid part can be written as

$$\bar{\boldsymbol{\sigma}}^{(f)} = 2\eta\bar{\boldsymbol{\gamma}} - \langle p_f \rangle \mathbf{1} - \varrho_f \langle \mathbf{u}' \otimes \mathbf{u}' \rangle, \quad (3.29)$$

where $\bar{\boldsymbol{\gamma}}$ denotes the averaged strain-rate tensor, $\langle p_f \rangle$ is the mean interstitial fluid pressure, ϱ_f is the fluid density, \mathbf{u}' refers to velocity fluctuations, and \otimes is the tensor product. We use brackets and the bar symbol to represent ensemble and volume-averaged quantities respectively. The ensemble average of a quantity $f(\mathbf{r}, t)$ at position \mathbf{r} and time t , is computed by performing a large number of experiments (“realizations”), with the same macroscopic initial and boundary conditions, and measuring f at \mathbf{r} at the same time relative to the beginning of each experiment. The average of these realizations forms the ensemble average. To do such a computation, we have to record the configuration C^N of N particles (specified by their positions, linear, and angular velocities) contained in a volume V . After calculating the probability $P(C^N, t)$ of observing a given configuration C^N at time t , we can define the ensemble average as $\langle f(\mathbf{r}, t) \rangle = \int P(C^N, t) f(\mathbf{x}, t; C^N) dC^N$. Such a definition is not very practical since it implies to specify the positions and velocities of all the particles contained in V . A strategy to bypass this difficulty is to focus on a single particle (“test particle”) and examine how other particles are distributed with respect to this particle. This leads to introduce the *pair distribution function* P_2 , which is the probability of finding a particle located at \mathbf{y} when the centre of the test particle is simultaneously in \mathbf{x} . Formulated in mathematical terms, this leads to write the ensemble average of $f(\mathbf{r}, t)$ as:

$$\langle f(\mathbf{r}, t) \rangle = \int_{C^2} P_2(t; \mathbf{x}, \mathbf{y}) f^{(2)}(\mathbf{x}, t; C^2) d\mathbf{x} d\mathbf{y} \approx \int_{C^2} P_2(t; \mathbf{x}, \mathbf{y}) f(\mathbf{x}, t) d\mathbf{x} d\mathbf{y} \quad (3.30)$$

where $f^{(2)}$ denotes the conditional averaged function when the position of two spheres is fixed. It is usually assumed that the conditional averaged function $f^{(2)}$ can be merely replaced by f . For dilute suspensions, apart from systems governed by fluctuations (critical phase transition), such an assumption is generally sound but remains to be proven for concentrated suspensions. The ensemble average is conceptually very convenient since it offers a sound statistical description of suspensions and it has the advantage that the operations of differentiation and ensemble averaging commute. However, its use is restricted by the poor knowledge that we may have on the distribution of particles in the suspension. An alternative is to use a volume average, that is, to average the quantity f over a control volume V , whose length scale must be large compared to the average distance between particles but small with respect to a distance over which the average of the property at hand varies appreciably. According we define the volume-averaged quantity \bar{f} as $\bar{f}(\mathbf{r}, t) = \int_V f(\mathbf{x}, t) d\mathbf{x} / V$.

In parallel to the fluid contribution, it is possible to obtain a generic expression of the particle contribution [40]:

$$\bar{\boldsymbol{\sigma}}^{(p)} = \bar{\boldsymbol{\sigma}}_{\text{surface}}^{(p)} - \frac{1}{2} J_p \langle \boldsymbol{\Omega}' \otimes \boldsymbol{\Omega}' \rangle - \rho_p \langle \mathbf{u}' \otimes \mathbf{u}' \rangle \quad (3.31)$$

where $\bar{\boldsymbol{\sigma}}_{\text{surface}}^{(p)}$ denotes the contribution due to forces exerted on the particle surface, $\boldsymbol{\Omega}'$ the fluctuations of angular velocity of particles, and J_p the inertia moment. It can be shown that the surface contribution $\bar{\boldsymbol{\sigma}}_{\text{surface}}^{(p)}$ reflects the effects of local forces at the particle level and may be deduced by averaging the local forces [40]:

$$\bar{\boldsymbol{\sigma}}_{\text{surface}}^{(p)} = \frac{a}{V} \sum_{m=1}^N \int_{A_p^{(m)}} \boldsymbol{\sigma} \mathbf{k} \otimes \mathbf{k} d\mathbf{k} = a n \langle \boldsymbol{\sigma} \mathbf{k} \otimes \mathbf{k} \rangle \quad (3.32)$$

where $\boldsymbol{\sigma} \mathbf{k}$ is the local stress acting on the particle surface ($\boldsymbol{\sigma} \mathbf{k} d\mathbf{k}$ is sometimes referred to as the contact force), \mathbf{k} is the outward normal at the contact point, $d\mathbf{k}$ the angle around \mathbf{k} , n is the number density ($n = \phi / (4\pi a^3 / 3)$). In the first equality in (3.32), we use a volume average of all contact forces acting on the surface $A_p^{(m)}$ of N beads included in a control volume V . The second equality is a simple translation of the first one in terms of ensemble average, which is more usual in kinetic theories or homogenization techniques.

To compute the two contributions, we have to introduce further ingredients. In particular, information on the particle distribution and the forces acting on particles is needed. In fact these two elements are tightly connected. It can be easily shown by first taking $f = 1$ in (3.30), then calculating the total time derivative that the pair distribution function satisfies an evolution equation called the Smoluchowski equation:

$$\frac{\partial P_2}{\partial t} + \nabla_{\mathbf{x}} \cdot P_2 \mathbf{U}_{\mathbf{x}}^{(2)} + \nabla_{\mathbf{r}} \cdot P_2 \mathbf{U}_{\mathbf{r}}^{(2)} = 0 \quad (3.33)$$

where $\mathbf{U}_{\mathbf{x}}^{(2)}$ and $\mathbf{U}_{\mathbf{r}}^{(2)}$ are the conditionally averaged velocity and relative velocity between the two particles located at \mathbf{x} and $\mathbf{x} + \mathbf{r}$. From a general point of view, these two velocities depend on the interparticle forces $\mathbf{F}^{(\text{hyd})}$, the Brownian motion, etc., which in turn depend on the imposed velocity gradient $\dot{\boldsymbol{\gamma}}$. There is no for-all-purpose solution to this equation, but several particular applications have been completely or partially explored. The simplest application of this theory is to consider suspensions sufficiently dilute for the hydrodynamic interplay between two particles to be negligible. In this case, if the Reynolds particle number $Re_p = 2\rho a |\mathbf{U}| / \eta$ (with \mathbf{U} the particle velocity relative to the fluid) comes close to zero, the hydrodynamic force that the particle undergoes is the Stokes force: $\mathbf{F}^{(\text{hyd})} = 6\pi\eta a \mathbf{U}$ [37]. (This force is inferred from the so-called Stokes equation, that is, the Navier–Stokes equation in which the inertial terms have been neglected since $Re_p \rightarrow 0$: $\mu \nabla^2 \mathbf{u} = \nabla p_f$.) Both the disturbances in the fluid velocity and fluid stress fields can be inferred from Stokes problem. At a point \mathbf{x} from the particle center, the disturbance in the fluid stress due to the slow motion

of the particle can be expressed as: $\boldsymbol{\sigma}^{(f)} = -\mathbf{x}\cdot\mathbf{f}/(4\pi|\mathbf{x}|^3)\mathbf{1} + \eta(\nabla\mathbf{u} + {}^t\nabla\mathbf{u})$, where $\mathbf{u} = (1 + \mathbf{x}\mathbf{x}/|\mathbf{x}|^2)\cdot\mathbf{f}/(8\pi\eta|\mathbf{x}|)$ is the disturbance in the velocity field and \mathbf{f} a constant such that $\int \boldsymbol{\sigma}^{(f)}\mathbf{k}\,d\mathbf{k} = \mathbf{F}^{(\text{hyd})}$ [37,50]. Using (3.32) with $P_2 = 1$ (assumption of dilute suspensions), we deduce that the bulk stress tensor can be expressed as:

$$\bar{\boldsymbol{\sigma}} = -\langle p_f \rangle \mathbf{1} + 2\eta \left(1 + \frac{5}{2}\phi \right) \bar{\boldsymbol{\gamma}}. \quad (3.34)$$

Thus the well-known Einstein relationship for the effective viscosity of a dilute suspension is obtained: $\eta_{eq}/\eta = 1 + 2.5\phi + \mathcal{O}(\phi)$, holding for solid fractions lower than 2%. This method has been progressively extended to take further interactions into account. Batchelor and Green [51,52] provided the pair distribution function and the disturbances in the velocity and pressure fields when the solid concentration is increased so that the velocity and pressure caused by the motion of a particle is significantly influenced by the presence of another particle. This leads to modifying the Einstein equation as follows: $\eta_{eq} = \eta + 2.5\phi + 7.6\phi^2 + o(\phi^2)$. Subsequently, the Brownian force [53], colloidal forces [54], the effect of solid fraction [55,56], and the particle surface roughness [57] have been included in the bulk stress computation.

3.4.2 Approximate Models

Because of the complexity of the dynamics of multiparticle interactions, rigorous microstructural theories generally do not provide analytical results. For instance, no analytical constitutive equation is available to predict the bulk behavior of Newtonian suspensions or granular flows at high solid fractions. A common way of overcoming this difficulty is to approximate the pair distribution function and the particle interaction expressions. This leads to a wide range of approximate models, whose applicability compensates for the introduction of *ad hoc* approximations. It is worth noting that numerical simulations of particle dynamics are increasingly used as an intermediate step between the theoretical models and the approximate equations. Typical examples include the treatment performed by Zhang and Rauenzahn [46,58] for granular flows and by Phan Thien [59,60] for concentrated viscous suspensions. Here, to exemplify the derivation of approximate models, we present the reasoning for deriving the bulk viscosity (see also [40,61]). The first step is to specify the approximate pair distribution function. This is usually done by considering a given configuration of particles (generally assumed to be cubic) and by assuming that the face-to-face distance between particles (ξ) is fixed on average and related to the solid fraction as follows:

$$\frac{\xi}{a} = 2\frac{\varsigma}{1-\varsigma}, \quad \text{with } \varsigma = 1 - \sqrt[3]{\frac{\phi}{\phi_m}}, \quad (3.35)$$

where ϕ_m is the maximum random solid concentration ($\phi_m \approx 0.635$ for unimodal suspensions of spherical particles). The pair distribution function may thus be

written as:

$$P_2(\mathbf{k})|_{r=\xi} = \sum_{i=1}^{n_c} \delta(\mathbf{k} - \mathbf{k}_i) , \quad (3.36)$$

where δ is the Dirac function, \mathbf{k}_i denotes the directions of the neighboring particle centers in the considered configuration with respect to the test-particle center, n_c the coordination number (number of indirect contacts). The lubrication force between two spheres can be divided into three contributions: a squeezing contribution, a shearing contribution, and a term due to the rotation of spheres. It can be shown that, in a steady state, the squeezing contribution is to leading order [62]:

$$\mathbf{F}_{\text{sq}} = \frac{3\pi}{2} \eta \frac{a^2}{\xi} \mathbf{c}_n , \quad (3.37)$$

where \mathbf{c}_n is the normal component of the relative particle velocity \mathbf{c} . The force due to shearing motion can be written to first order: $\mathbf{F}_{\text{sh}} = \pi\eta a \ln(\xi/a) \mathbf{c}_t$ (with \mathbf{c}_t the tangential component of the relative particle velocity) and the force due to the rotation of particles is: $\mathbf{F}_{\text{rot}} = 2\pi\eta a^2 \ln(\xi/a) \mathbf{k} \times \boldsymbol{\Omega}$. These two contributions are of the same order and their magnitudes increase as $\ln(\xi/a)$. Consequently, for concentrated suspensions, to leading order in ξ/a , they are negligible compared to the squeezing force. All the above expressions tend toward infinity when the gap becomes extremely small, which would preclude any direct contact. The squeezing contribution can be evaluated by incorporating (3.37) into (3.32):

$$\boldsymbol{\sigma}_{\text{sq}}^{(p)} = \frac{3\pi}{2} \frac{a^3}{\xi} \mu n_d \langle \mathbf{c}_n \otimes \mathbf{k} \rangle . \quad (3.38)$$

The relative velocity is computed as the average velocity imposed by the bulk flow:

$$\mathbf{c} \approx 2a\bar{\mathbf{L}}\mathbf{k} - 2a \langle \boldsymbol{\Omega} \rangle \times \mathbf{k} = 2a(\bar{\boldsymbol{\gamma}}\mathbf{k} - (\langle \boldsymbol{\Omega} \rangle - \bar{\boldsymbol{\omega}}) \times \mathbf{k}) , \quad (3.39)$$

where $\bar{\mathbf{L}} = \nabla \bar{\mathbf{u}}$ denotes the bulk velocity gradient, $\bar{\boldsymbol{\omega}}$ is the curl of $\bar{\mathbf{L}}$, and $\bar{\boldsymbol{\gamma}}$ is the symmetric part of $\bar{\mathbf{L}}$. It follows that the squeezing velocity can be written:

$$\mathbf{c}_n = 2a(\bar{\boldsymbol{\gamma}} : \mathbf{k} \otimes \mathbf{k})\mathbf{k} . \quad (3.40)$$

The contribution due to the squeezing motion is directly deduced from (37):

$$\boldsymbol{\sigma}_{\text{sq}}^{(p)} = \frac{9}{4} \frac{a}{\xi} \eta \phi(\bar{\boldsymbol{\gamma}} : \mathbf{k}_i \otimes \mathbf{k}_i) \mathbf{k}_i \otimes \mathbf{k}_i . \quad (3.41)$$

It should be noted that the Newtonian character of bulk stress is dictated by the symmetry of the directions \mathbf{k}_i with respect to the principal directions of the strain-rate tensor. Let us consider a simple shear flow. If we assume that (i) the particle configuration is cubic, (ii) its privileged axes coincide with the principal axes of the strain-rate tensor, (iii) the predominant action is due to squeezing, then we can deduce that the bulk viscosity varies as:

$$\eta_{\text{eq}} = \alpha \frac{a}{\xi} \eta , \quad (3.42)$$

with $\alpha = 9\phi/4$. Thus it is shown that the bulk viscosity of a concentrated suspension should tend towards infinity when the solid concentration comes closer to its upper limit ϕ_m .

The main drawback in the derivation of approximate models lies in the speculative character of many assumptions. As pointed out by different authors [63,64], the mean-field approach presented here suffers a great deal from questionable approximations. Among others, it is obvious from (3.40)–(3.41) that the resulting bulk stress tensor depends to a large extent on the particle arrangement, the face-to-face distance between particles, and the velocity field. For instance, using different methods or assumptions, most authors have obtained a bulk viscosity whose expression is structurally similar to (3.42), but sometimes with a different value for α . For instance, using a similar approach, Goddard [65] found $\alpha = 3\phi/8$ while van den Brule and Jongshaap arrived at $\alpha = 9\phi/4$ [61]. Using an energy-based method, Frankel and Acrivos obtained $\alpha = 9/4$ [66]. Sengun and Probstein [67] inferred a more complicated expression from energy considerations but, asymptotically for solid concentrations near the maximum concentration, they found a comparable expression for the bulk viscosity, with $\alpha \approx 3\pi/4$, close to the value determined by Frankel and Acrivos. On the basis of energy and kinematic considerations, Marrucci and Denn [64] argued that coefficient α is not constant and must vary as $\alpha \propto \ln(a/\xi)$ in the worst case. Likewise, Adler et al. [63] put forward that averaging the different configurations through which the particle arrangement passes does indeed smooth the singularity $1/\zeta$ and consequently the bulk viscosity does not diverge when the solid concentration tends to its maximum.

It is worth noting that approximate models can be built using empirical reasoning without any recourse to a detailed analysis of particle interactions. A typical example in the area of suspensions is given by Krieger and Dougherty's model [68]. The authors assumed that within a suspension of non-Brownian, noncolloidal particles, a particle sees a homogeneous fluid surrounding it, whose viscosity depends only on the solid fraction and the interstitial fluid viscosity. This is obviously a crude assumption since this particle is more influenced by nearby particles than by more distant particles. Using dimensional analysis (see below), it may be shown that the bulk viscosity is of the form: $\eta_{\text{eq}} = \eta f(\phi)$. The bulk viscosity can be computed by assuming that one first introduces a solid fraction ϕ_1 , then a solid fraction ϕ_2 so that the resulting solid concentration is ϕ . For doing so, we must choose ϕ_2 such that it satisfies: $\phi_2 = (\phi - \phi_1)/(1 - \phi_1)$. Finally we must have: $f(\phi_1)f(\phi_2) = f(\phi)$, which must hold whatever the solid fractions. It can be shown that the only function obeying such an equality is of the form: $f(\phi) = (1 - \phi)^{-\beta}$. Experimentally, β has been generally estimated at approximately 2. Krieger and Dougherty's expression has been modified to represent experimental data over as wide a range of solid concentrations as possible:

$$\frac{\eta_{\text{eq}}}{\eta} = \left(1 - \frac{\phi}{\phi_m}\right)^{-[\eta]\phi_m}, \quad (3.43)$$

where $[\eta] = \lim_{\phi \rightarrow 0} (\eta_{\text{eq}} - \eta)/(\eta\phi) = 2.5$ is called the *intrinsic viscosity*. Such a relation matches the Einstein expression at low solid fractions. Many expressions with a form similar to (3.43) have been proposed to take further phenomena (aggregating of particles [69], shear-thinning, colloidal effects, polydispersity [70,71], etc.) into account. A common element in several models is to consider that the maximum solid concentration is not constant but is rather a shear-rate-dependent function since it should reflect changes in the microstructure. For instance, in order to make an allowance for viscoplastic behavior, Wildemuth and Williams [73,72] have assumed that the maximum solid fraction relaxes with shear stress from a lower value ϕ_0 to an upper bound ϕ_∞ :

$$\frac{1}{\phi_m} = \frac{1}{\phi_0} - \left(\frac{1}{\phi_0} - \frac{1}{\phi_m} \right) f(\tau) \quad (3.44)$$

where $f(\tau) = (1 + A\tau^{-m})^{-1}$, A and m are two constants intrinsic to the material. This also implies that such a suspension (with $\phi_0 \leq \phi \leq \phi_\infty$) exhibits a yield stress:

$$\tau_c(\phi) = \left[A \left(\frac{\phi/\phi_0 - 1}{1 - \phi_m/\phi_\infty} \right) \right]^{1/m}. \quad (3.45)$$

It should be noted that in the model and experiments presented by Wildemuth and Williams, the yield appearance reflects either colloidal effects or structural changes in the particle arrangement (jamming, friction between coarse particles) or both of them.

In contrast, Sengun and Probstein [67] proposed different arguments to explain the viscoplastic behavior observed in their investigations on the viscosity of coal slurries (with particle size typically ranging from $0.4 \mu\text{m}$ to $300 \mu\text{m}$). Their explanation consists of two approximations. First, as it is the interstitial phase, the dispersion resulting from the mixing of fine colloidal particles and water imparts most of its rheological properties to the entire suspension. Secondly, the coarse fraction is assumed to act independently of the fine fraction and to enhance the bulk viscosity. They introduced a *net viscosity* η_{nr} of a bimodal slurry as the product of the fine relative viscosity η_{fr} and the coarse relative viscosity η_{cr} . The fine relative viscosity is defined as the ratio of the apparent viscosity of the fine-particle suspension to the viscosity of the interstitial fluid: $\eta_{\text{fr}} = \eta_f/\eta_0$. The coarse relative viscosity is defined as the ratio of the apparent viscosity of the coarse-particle slurry to the viscosity of the fine-particle suspension: $\eta_{\text{cr}} = \eta_c/\eta_f$. The two relative viscosities depend on the solid concentrations and a series of generalized Péclet numbers. For the coarse-particle suspensions, all the generalized Péclet numbers are much greater than unity. Using a dimensional analysis, Sengun and Probstein deduced that the coarse relative viscosity cannot depend on the shear rate. In contrast, bulk behavior in fine-particle suspensions is governed by colloidal particles and thus at least one of the generalized Péclet numbers is of the order of unity, implying that the fine relative viscosity is shear-dependent. Sengun and Probstein's experiments on viscosity of coal slurries confirmed the reliability of this concept [67]. Plotting $\log \eta_{\text{nr}}$ and $\log \eta_{\text{fr}}$

against $\log \dot{\gamma}$, they found that over a wide range of concentrations, the curves were parallel and their distance was equal to $\log \eta_{cr}$ (see Fig. 3.7). However, for solid concentrations in the coarse fraction exceeding 0.35, they observed a significant departure from parallelism which they ascribed to nonuniformity in the shear rate distribution within the bulk due to squeezing effects between coarse particles.

Generally, all these empirical models successfully provide an estimation of bulk viscosity over a wide range of solid fraction, as shown in Fig. 3.8, provided that the maximum solid concentration has been correctly evaluated. In practice, for natural fluids such as debris suspensions, this evaluation may be problematic and lead to a large uncertainty in computing bulk viscosity.

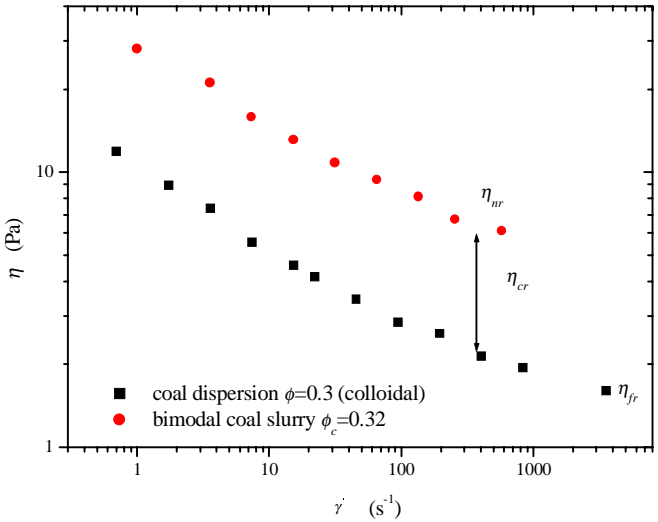


Fig. 3.7. Variation of the bulk viscosity of coal slurry as a function of the shear rate. The bulk viscosity curve is parallel to the curve obtained with the fine fraction. After [67]

3.4.3 Contribution of Dimensional Analysis

Expressing bulk behavior in terms of dimensionless groups is a practical and usual way of identifying the most relevant variables and delineating flow regimes. A certain number of studies have so far focused on suspensions of rigid spherical particles within a Newtonian fluid with a narrow size distribution [7,54,76,78]. In this case, a suspension of noninteracting particles is characterized by eight variables: (i) for particles, the density ρ_p , the radius a , and the solid volume concentration ϕ ; (ii) for the interstitial fluid, the viscosity η and the density ρ_f ; (iii) for the conditions imposed during an experiment, the temperature T , the

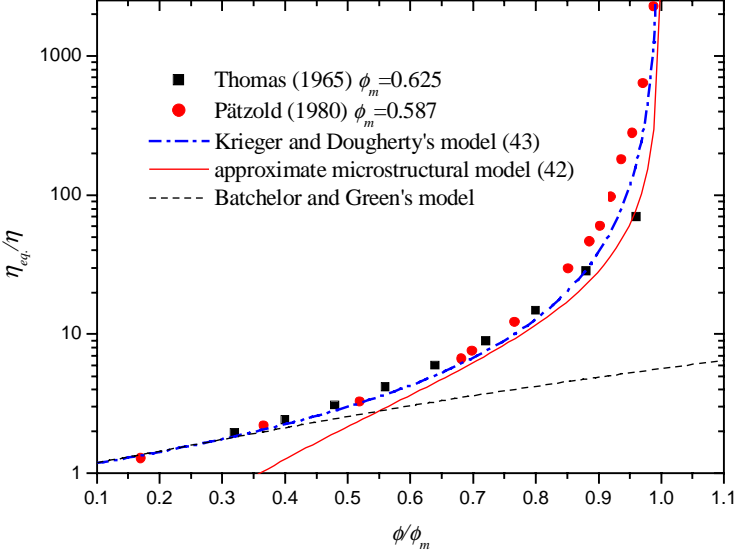


Fig. 3.8. Variation in the bulk viscosity as a function of the reduced fraction. Typical data obtained by Thomas [74] and Pätzold [75] are reported

shear rate $\dot{\gamma}$ (or equivalently the shear stress τ), and the experiment duration t_{exp} . According to the principles of dimensionless analysis, the bulk viscosity can be expressed as a function of $8 - 3 = 5$ dimensionless groups. The following numbers are preferentially formed: the solid fraction ϕ , the *Reynolds particle number* $Re = (2a)^2 \dot{\gamma} / \eta$ reflecting fluid inertia at the particle scale, the *Péclet number* $Pe = 6\pi \dot{\gamma} a^3 \eta / (kT)$ (where k refers to the Boltzmann constant) defined as the ratio of viscous forces to Brownian forces, the *Deborah number* expressed as the ratio of a particle relaxation time t_p to the typical time of the experiment $De = t_p / t_{\text{exp}}$ (depending on the particle size, the particle relaxation can be linked to the Brownian diffusion time $t_p = 6\pi a^3 \eta / (kT)$ or the Stokes relaxation time $t_p = 2a^2 \rho_p / (9\eta)$), the *Stokes number* $St = 2\rho_p Re / (9\rho_f)$ defined as the ratio of a particle relaxation time to a fluid characteristic time. If the particles are colloidal, van der Waals' attraction and electrostatic repulsion must be taken into account, giving rise to two dimensionless groups: an attraction number $N_{\text{att}} = \eta a^3 \dot{\gamma} / A$, where A is the Hamaker constant of the colloidal particles, and a repulsion number $N_{\text{rep}} = \eta a^2 \dot{\gamma} / (\varepsilon \psi_0^2)$, where ε is the fluid permittivity and ψ_0 the surface potential. As examples, taking $a = 0.5 \text{ mm}$, $\dot{\gamma} = 1 \text{ s}^{-1}$, $\eta = 10^{-3} \text{ Pa}\cdot\text{s}$, $t_{\text{exp}} = 10 \text{ s}$, $T = 293 \text{ K}$, $\rho_p = 2500 \text{ kg/m}^3$ for a suspension of coarse particles slowly sheared (typically a suspension of particles in a water-glycerol solution), we find: $Re = 10^{-3}$, $Pe = 580 \cdot 10^6$, $St = 5 \cdot 10^{-4}$, $De = 10^{-2}$. Taking $a = 0.5 \mu\text{m}$, $A \approx 10^{-20} \text{ J}$, $\varepsilon = 7 \cdot 10^{-10} \text{ C}^2 \text{J}^{-1} \text{m}^{-1}$, $\psi_0 \approx 100 \text{ mV}$, $\rho_p = 2650 \text{ kg/m}^3$ for a suspension of colloidal particles slowly sheared (typically a water-kaolin dispersion), we find: $Re = 10^{-9}$, $Pe = 0.6$, $St = 6 \cdot 10^{-10}$,

$De = 6 \cdot 10^{-2}$, $N_{\text{att}} \approx 10^{-2}$, $N_{\text{rep}} \approx 4 \cdot 10^{-5}$. Using the dimensional analysis principles (i.e. ignoring dimensionless numbers much lesser or greater than unity) [79], we expect from the magnitude orders found above that, typically for the viscosity of a coarse-particle suspension, bulk viscosity depends on the solid concentration mainly: $\eta_{\text{eq}}/\eta = f(\phi)$, and for a dispersion, it depends on the Péclet number and the solid concentration: $\eta_{\text{eq}}/\eta = f(\phi, Pe)$. Such scalings have been successfully compared to experimental data [80,81]. The main problem encountered in geophysics is that fluids generally involve a wide range of size particles and different types of particle interaction. For instance, typically for a debris flow, the particle size ranges from $1 \mu\text{m}$ to more than 1m and particle interactions can include colloidal effects, collisional, frictional, lubricated contacts, etc. Thus the large number of physical parameters intervening in the problem makes any thorough and general examination of the resulting flow regimes intricate. To our knowledge, only partial results have so far been provided on the relevant dimensionless groups controlling bulk behavior of natural fluids [7] (see also Chap. 21).

References

1. H.A. Barnes, J.F. Hutton, K. Walters: *An introduction to rheology* (Elsevier, Amsterdam 1997)
2. R.I. Tanner: *Engineering Rheology* (Clarendon Press, Oxford 1988)
3. G.V. Middleton, P.R. Wilcock: *Mechanics in the Earth and Environmental Sciences* (Cambridge University Press, Cambridge 1994)
4. B.D. Coleman, H. Markowitz, W. Noll: *Viscometric flows of non-Newtonian fluids* (Springer, Berlin 1966)
5. K. Walters: *Rheometry* (Chapman and Hall, London 1975)
6. R.B. Bird, R.C. Armstrong, O. Hassager: *Dynamics of polymeric liquids* (John Wiley & Sons, New York 1987)
7. P. Coussot, C. Ancey: *Rhéophysique des pâtes et des suspensions* (EDP Sciences, Les Ulis 1999) (in French)
8. J.F. Steffe: *Rheological methods in food process engineering* (Freeman Press, East Lansing, USA 1996). Free sample available at: <http://www.egr.msu.edu/~steffe/freebook/offer.html>
9. Y. Wang, K. Hutter: *Granular Matter* **1**, 163 (1999)
10. K. Hutter, B. Svendsen, D. Rickenmann: *Continuum Mech. Therm.* **8**, 1 (1996)
11. I. Vardoulakis, J. Sulem: *Bifurcation Analysis in Geomechanics* (Blackie Academic & Professional, Glasgow 1995)
12. A. Bedford, D.S. Dumbeller: *Int. J. Eng. Sci.* **21**, 863 (1983)
13. S. Chapman, T.G. Cowling: *The mathematical theory of nonuniform gases* (Cambridge University Press, Cambridge 1970)
14. J.T. Jenkins, H.M. Hanes: *J. Fluid Mech.* **370**, 29 (1998)
15. S.B. Savage: 'Marginal ice zone dynamics modelled by computer simulations involving floe collisions'. In: *Mobile particulate systems, Carghese, 1994*, ed. by E. Guazelli and L. Oger (Kluwer Academic Publishers, Dordrecht 1995); S.B. Savage, G.B. Crocker, M. Sayed, T. Carrieres, *Cold Reg. Sci. Technol.* **31**, 163 (2000)
16. S.B. Savage: 'Flow of granular materials'. In: *Theoretical and Applied Mechanics*, ed. by P. Germain, J.-M. Piau, D. Caillerie (Elsevier, Amsterdam 1989)

17. C. Ancey, P. Coussot, P. Evesque: *Mech. Cohes. Frict. Mat.* **1**, 385 (1996)
18. C. Ancey, P. Evesque: *Phys. Rev. E* **62**, 8349 (2000)
19. A. Borgia, F.J. Spera: *J. Rheol.* **34**, 117 (1990)
20. T.M.T. Yang, I.M. Krieger: *J. Rheol.* **22**, 413 (1978)
21. I.M. Krieger: *Trans. Soc. Rheol.* **12**, 5 (1968)
22. Q.D. Nguyen, D.V. Boger: *Ann. Rev. Fluid Mech.* **24**, 47 (1992)
23. P. Coussot, J.M. Piau: *Rheol. Acta* **39**, 105 (1995)
24. Y.L. Yeow, W.C. Ko, P.P.P. Tang: *J. Rheol.* **44**, 1335 (2000)
25. Y.T. Nguyen, T.D. Vu, H.K. Wong, Y.L. Yeow: *J. Non-Newtonian Fluid Mech.* **87**, 103 (1999)
26. H.A. Barnes, J.O. Carnali: *J. Rheol.* **34**, 851 (1990)
27. C.J. Phillips, T.R.H. Davies: *Geomorphology* **4**, 101 (1991)
28. N. Pashias, D.V. Boger: *J. Rheol.* **40**, 1179 (1996)
29. P. Coussot, S. Proust, C. Ancey: *J. Non-Newtonian Fluid Mech.* **66**, 55 (1996)
30. R.W. Griffith: *Ann. Rev. Fluid Mech.* **32**, 477 (2000)
31. O. Pouliquen: *Phys. Fluids* **11**, 542 (1999)
32. A.M. Johnson, J.R. Rodine: 'Debris flow'. In: *Slope Instability*, ed. by D. Brundsen, D.B. Prior (John Wiley & Sons, Chichester 1984)
33. I. Newton: *Philosophiæ naturalis principia mathematica*. English translations of this historical text are available, e.g. F. Cajori: *Sir Isaac Newton's mathematical principles of natural philosophy and his system of the world* (University of California Press, Berkeley 1962)
34. F.T. Trouton, E.S. Andrews: *Phil. Mag.* **7**, 347 (1904). F.T. Trouton: *Proc. Roy. Soc. London Ser. A* **77**, 426 (1906)
35. R.B. Bird, G.C. Dai, B.J. Yarusso: *Rev. Chem. Eng.* **1**, 1 (1983)
36. J.D. Sherwood, D. Durban: *J. Non-Newtonian Fluid Mech.* **77**, 155 (1998)
37. G.K. Batchelor: *An introduction to fluid mechanics* (Cambridge University Press, Cambridge 1967)
38. R. Hill: *Mathematical theory of plasticity* (Oxford University Press, Oxford 1950)
39. C.S. Campbell: *Ann. Rev. Fluid Mech.* **22**, 57 (1990)
40. C. Ancey, P. Coussot, P. Evesque: *J. Rheol.* **43**, 1673 (1999)
41. G.K. Batchelor: *Ann. Rev. Fluid Mech.* **6**, 227 (1974)
42. R. Herczynski, I. Pienkowska: *Ann. Rev. Fluid Mech.* **12**, 237 (1980)
43. R.J.J. Jongschaap, D. Doeksen: *Rheol. Acta* **22**, 4 (1983)
44. M. Lätzel, S. Luding, H.J. Herrmann: *Granular Matter* **2**, 123 (2000)
45. D.Z. Zhang, A. Prosperetti: *Int. J. Multiphase Flow* **23**, 425 (1997)
46. D.Z. Zhang, R.M. Rauenzahn: *J. Rheol.* **41**, 1275 (1997)
47. B. Cambou, P. Dubujet, F. Emeriault, F. Sidoroff: *Eur. J. Mech. A/Solids* **14**, 255 (1995)
48. Y.A. Buyevich, I.N. Shchelchkova: *Prog. Aero. Sci.* **18**, 121 (1978)
49. G.K. Batchelor: *J. Fluid Mech.* **41**, 545 (1970)
50. S. Kim, S.J. Karrila: *Microhydrodynamics: principles and selected applications* (Butterworth-Heinemann, Stoneham 1991)
51. G.K. Batchelor, J.T. Green: *J. Fluid Mech.* **56**, 401 (1972)
52. G.K. Batchelor, J.T. Green: *J. Fluid Mech.* **56**, 375 (1972)
53. G.K. Batchelor: *J. Fluid Mech.* **83**, 97 (1977)
54. W.B. Russel, D.A. Saville, W.R. Schowalter: *Colloidal dispersions* (Cambridge University Press, Cambridge 1995)
55. J.F. Brady, J.F. Morris: *J. Fluid Mech.* **348**, 103 (1997)
56. R.A. Lionberger, W.B. Russel: *J. Rheol.* **41**, 399 (1997)

57. H.J. Wilson, R.H. Davis: *J. Fluid Mech.* **421**, 339 (2000)
58. D.Z. Zhang, R.M. Rauenzahn: *J. Rheol.* **44**, 1019 (2000)
59. N. Phan-Thien, X.-J. Fan, B.C. Khoo: *Rheol. Acta* **38**, 297 (1999)
60. N. Phan-Thien: *J. Rheol.* **39**, 679 (1995)
61. B.H.A.A. van den Brule, R.J.J. Jongshaap: *J. Stat. Phys.* **62**, 1225 (1991)
62. R.G. Cox: *Int. J. Multiphase Flow* **1**, 343 (1974)
63. P.M. Adler, M. Zuzovski, H. Brenner: *Int. J. Multiphase Flow* **11**, 387 (1985)
64. G. Marrucci, M. Denn: *Rheol. Acta* **24**, 317 (1985)
65. J.D. Goddard: *J. Non-Newtonian Fluid Mech.* **2**, 169 (1977)
66. N.A. Frankel, A. Acrivos: *Chem. Eng. Sci.* **22**, 847 (1967)
67. M.Z. Sengun, R.F. Probstein: *Rheol. Acta* **28**, 382 (1989)
68. I.M. Krieger, T.J. Dougherty: *Trans. Soc. Rheol.* **3**, 137 (1959)
69. C. Tsenoglou: *J. Rheol.* **34**, 15 (1990)
70. C. Chang, R.L. Powell: *J. Rheol.* **38**, 85 (1994)
71. P. Gondret, L. Petit: *J. Rheol.* **41**, 1261 (1997)
72. C.R. Wildemuth, M.C. Williams: *Rheol. Acta* **23**, 627 (1984)
73. C.R. Wildemuth, M.C. Williams: *Rheol. Acta* **24**, 75 (1985)
74. D.G. Thomas: *J. Colloid Sci.* **20**, 267 (1965)
75. R. Pätzold: *Rheol. Acta* **19**, 322 (1980)
76. I.M. Krieger: *Adv. Colloid. Interface Sci.* **3**, 111 (1972)
77. P. Coussot, C. Ancey: *Phys. Rev. E* **59**, 4445 (1999)
78. A.I. Jomha, A. Merrington, L.V. Woodcock, H.A. Barnes, A. Lips: *Powder Tech.* **65**, 343 (1990)
79. G.I. Barenblatt: *Scaling, self-similarity, and intermediate asymptotics* (Cambridge University Press, Cambridge 1996)
80. W.B. Russel: *J. Rheol.* **24**, 287 (1980)
81. J.C. van der Werff, V.F. de Kruij: *J. Rheol.* **33**, 421 (1989)